Effect of shear flow on spherulitic growth and nucleation rates of Polypropylene

Felice De Santis, Roberto Pantani, Giuseppe Titomanlio

Department of Industrial Engineering, University of Salerno, 84084 Fisciano (SA), Italy

Felice De Santis
University of Salerno,
Department of Industrial Engineering,
Via Giovanni Paolo II, 132 - 84084 - Fisciano (SA)
E-mail: fedesantis@unisa.it
Phone: +39 089 96 4013

Abstract

The effect of flow on the crystallization kinetics of polymers is well known, at least from a qualitative point of view. Quantitative determinations are difficult to obtain, due to the experimental difficulties of obtaining direct measurements of nucleation and growth rates during flow. In this work, step shear tests were conducted in the Linkam device adopting a new protocol in which the flow is applied when the crystalline structures have already reached dimensions easily detectable by an optical microscope. This *delayed* protocol allowed to achieve a more accurate experimental analysis of the effect of flow on spherulite growth rate with respect to what already reported in the literature. The new results obtained for the growth rate were interpreted, with the equilibrium melting temperature function of the shear rate. Also the nucleation rate could be assessed and the existence of a correlation between nucleation rate and growth rate was confirmed.

Keywords

Nucleation and growth rates – Shear Flow – Polypropylene

Introduction

Semicrystalline polymers are highly versatile because of their tunability: changes of the processing conditions, which modify the thermomechanical history up to solidification, give rise to changes of characteristics, dimensions, and spatial organization of crystallites (in a single word the morphology) and thus influence material properties such as strength, hardness, permeability, surface texture, transparencies and almost every functional property [1-3]. Indeed, in the last decades large attention was devoted by researchers to investigate the main aspects of the transport phenomena, like heat transfer, flow and crystallization kinetics during processing of thermoplastic polymers [4].

The intrinsic interconnection among these transport phenomena determines objective difficulties to realize a direct and local measurement of the effect of the flow during the processing. As an example, if it is possible to measure nucleation density and growth rate of spherulitic structure in a narrow range of temperature [5]; when flow is applied, quantitative experiments are even more complex and limited. Sometimes, to overcome these difficulties, structure development is analyzed by their interactions with electromagnetic waves (from infrared to X-rays [6]), but this indirect evidence of crystallization must then be interpreted.

Prof. Janeschitz-Kriegl, in his monograph on "Crystallization Modalities in Polymer Melt Processing" [4], dedicates a chapter to flow induced processes causing oriented crystallization, with an interesting historical review. Starting from papers in the seventies, the effects of shear flow [7] and extensional flow [8] were investigated. Parallel plate rotational rheometers were adopted for early studies [9, 10], but also more recently in [11-18], using the apparatus of Linkam Scientific Instruments to study the huge effect of the flow on the acceleration of crystallization rate.

Rotational instruments are intrinsically limited to low shear rate, if compared to some processing conditions, so duct flow experiments were set up in novel instruments at Caltech [19-23] and at TU/e [24-28], developing the Cambridge Multipass Rheometer [29, 30].

Even if the effect of the flow on solidification is widely known, in situ measurement during flow is still not common: the mainstream is to observe the outcome after the application of a shear step [31].

Starting from quiescent measurements of solidified i-PP samples (aka *post mortem*) [32] and optical measurement during fast cooling [33], a large effort in the characterization of all aspects of a specific resin, a commercial grade with tradename Moplen T30G, was spent by the Polymer Technology Group at University of Salerno. In particular, to model the morphology evolution in the injection molding process, the effect of the flow on the crystallization kinetics of this i-PP was analyzed [34-37]. In particular, some measurements were performed of nucleation density and growth rate of spherulites [37] in the Linkam device, under continuous shear in a range of temperatures (138÷144°C) and shear rates ($0 \div 0.30\ s^{-1}$).

Pantani et al. [37] suggested a correlation between nucleation rate and spherulitic growth rate at low shear rate: whatever the controlling mechanism for the enhancement of nucleation rate is, it has a similar effect also on growth rate. The effect of flow on nucleation and growth rates was attributed to the increase of the equilibrium melting temperature due to flow. In turn, the equilibrium melting temperature estimated for the tests conducted in the whole range of temperatures and shear rates was found to be dependent on the Weissenberg number.

Starting from these experiences, in this work step shear rate experiments were carried out in the Linkam shear cell changing shearing time, and analyzing the resulting morphology of the section of the solidified sample. Furthermore, a new method to investigate the effect of shear rate on growth rate was presented, expanding the previous range of shear rate of one order of magnitude.

Experimental

Material

An isotactic polypropylene was adopted in this work. It is a commercial grade of i-PP supplied by Montell (Ferrara, Italy), with the tradename of Moplen T30G, and it is a general-purpose homopolymer for extrusion/molding applications, with a melt flow index equal to 3.6 (ASTM D1238/L). The molecular weight distribution was determined by a size exclusion chromatography as weight-average molar mass M_w of 376 kg mol^{-1}, polydispersity index M_w/M_n of 6.7, and meso pentads content 87.6%. The glass transition temperature (T_g) and the glass and melting temperatures of Moplen T30G reported on the material datasheet are -15°C and 166°C, respectively.
The effect of the flow applied during crystallization on the morphology evolution and the crystallization kinetics of the same resin have been already explored [36-38] to some extent.

Optical Shearing Cell

The Linkam CSS-450 temperature optical shear stage, with a maximum sample diameter of 30 mm, coupled with an optical polarizing microscope, Olympus BX41 model using 10× M PLAN Objective, was employed for the observation of the crystallization process under a shear field, through a fixed circular window (viewing area 2.8 mm diameter) at the radial distance of R_{window}=7.5 mm from the center [37, 39].
The Linkam shear stage has two quartz plates: the top plate is fixed while the bottom one can rotate to produce a shear field. The sample is held in the gap between the two plates. The mechanical design of the hot stage provides control over various parameters of the shear experiment, such as temperature, cooling/heating rate, gap thickness, shear strain rate and duration as well as the shear mode such as steady, step and oscillatory. In all the experiments reported in this work, the step mode was selected. Since in plate-plate configuration the gap is a constant between the top and the bottom plates there is a radial distribution of the shear rates. In particular, the shear rate, $\dot{\gamma}$, is related to shear rate at the observation window, $\dot{\gamma}_{window}$, as

$$\dot{\gamma} = \left(R/R_{window}\right) \times \dot{\gamma}_{window} \quad (1)$$

where R is the radial position.
Digital images have been recorded, during crystallization, using a CCD camera (3.3 MP, Olympus ColorView II) and software (Olympus AnalySIS 3.2). Quantitative analysis of the digital images have been carried out using suitable software (ImageJ, a public domain, image processing software developed at the National Institutes of Health).
The growth rate was measured by monitoring the radius of the spherulites during time. As far as the nucleation rate is concerned, from the images acquired at the optical window the number of spherulites in the visible field was measured after the end of the step shear when the spherulites are visible. Knowing the area of the image (385000 μm^2) and the focal depth (80 μm), also the number N_V of spherulites per unit volume can be calculated.

Methods

The samples (initially in the form of pellets) were placed between the top and the bottom of cleaned quartz plates of the Linkam shear cell at room temperature. The samples were then heated to 210°C and as soon as the samples were completely melted, the gap between the quartz plates was reduced, by slowly lowering the upper plate. In all the performed experiments the gap was set to 500 μm.

The crystallization kinetics were investigated starting from the molten amorphous material, after holding the sample at 210°C for 20 minutes in order to erase the effect of previous thermo-mechanical history. The gap was set to the chosen value of 500 μm and the sample was cooled at 10 K min^{-1} from 210°C directly to the isothermal test temperature 140°C (crystallization temperature).

The crystallization temperature (140°C) was selected so to have crystallization times of the order of 10^4 s under quiescent conditions, on the basis of previous works [5, 32]. In the same works, it was verified that the adopted protocol preserves the material properties minimizing the effect of surface nucleation and thermo-mechanical degradation.

Two different experimental protocols were adopted:

- the shear step was applied 1 minute after reaching 140°C; in this work this protocol is called "*immediate*";
- the sample was kept quiescent at 140°C for about 20 min, then a shear step was applied, as sketched in the inset of Fig. 1; in this work this protocol is called "*delayed*".

The "*immediate*" shear step protocol was already adopted [37, 40] to characterize the material studied in this work at different temperatures and at shear rates lower than 0.3 s^{-1} by measuring on line the nucleation and growth rates of spherulites.

In that case the shear step was kept until a considerable value of crystallinity was reached, being indeed a continuous shear experiment. This method does not allow to measure the growth rate at higher shear rates because of two main reasons: the spherulites move very fast through the observation window, and thus the measurements of the radii can be carried out only during short time intervals; furthermore, the spherulites are small thus impeding a reliable measurement of their radius.

The step shear rate experiments according to the *immediate* protocol were performed imposing a nominal shear rate of 5 s^{-1}, at the optical window, with shearing time of 10 s, 20 s, 30 s, and 40 s.

In a similar way, the experiments according to the *delayed* protocol were performed exploring some "couples" of shear rate and shearing time, as summarized in Table 1.

Table 1. Settings for *delayed* protocol experiments

Nominal shear rate [s^{-1}]	Shearing time [s]
2	10
3	10
5	10
0.5	40
2	40
2	60

With both protocols (*immediate* and *delayed*), after shear cessation, the material was kept at 140°C for 4 hours, to let it completely crystallize under isothermal conditions [5].

The sample was than cooled down to room temperature, taken out from the shearing cell and its thickness was measured. Since the final thickness of the sample could be slightly different from the set 500 μm, the shear rate was corrected accordingly.

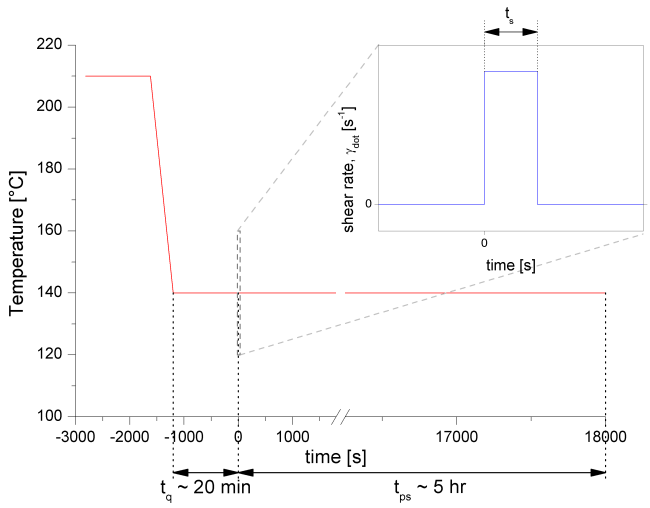

Fig. 1. Schematics diagram of the *delayed* experimental protocol, delayed step shear: temperature evolution and, in the insert, step shear evolution after partial quiescent crystallization.

Results

As introduced in the Methods section, two experimental protocols were adopted in this work: *immediate* and *delayed* step shear rate. These protocols give important and complementary information of crystalline structure formation during shear flow.

Immediate step shear rate experiments at 140°C

During the *immediate* shear step experiments, the samples were monitored through the optical window, and during the application of the shear step there was not any evidence of the formation of new structures: the shearing times (adopted for the steps) were not sufficient for the growth of crystalline structures at the microscopic observation scale, in spite of the enhancement effect of the flow on growth rate.

With sufficient amount of time after the end of the shear step, several spherulites appeared as shown in Fig. 2. Continuous shear experiments were performed in a previous work [37] but only moderate shear rates could be applied: at large shear rates the nuclei density becomes enormous before the spherulites become large enough to be measurable using the optical microscopy.

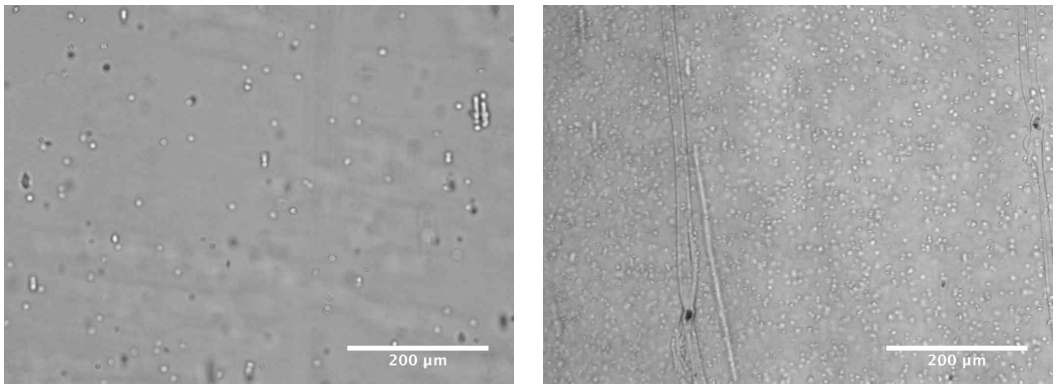

Fig. 2 Optical micrograph of samples during crystallization: shear rate 5 s^{-1}, shearing time 10 s (left) and 40 s (right).

Also the morphology of the final samples was analyzed after solidification. Since the shear rate increases proportionally to the radius of the plate, a correspondent change of morphology along the radius was expected for each shearing time along the maximum diameter, as shown in Fig. 3; the slices were cut through the whole cross section, using a Leica RM2265 microtome.

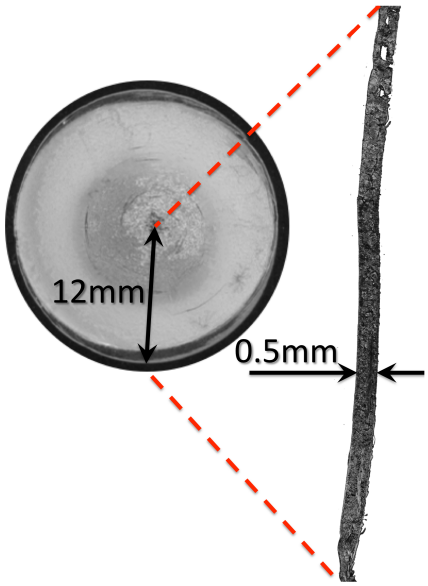

Fig. 3 On the left, the sample (disk) after solidification: shear rate 5 s^{-1} imposed, at radius 7.5 mm, with the *immediate* protocol, shearing time 10 s; the black solid line corresponds to the section plane. On the right, polarized optical micrograph of the section.

The Multiple Image Alignment (Olympus MIA module) was used to assemble a high resolution image of the whole cross section, long about 12 mm as the sample radius in Fig. 3 and wide about 0.5 mm as the sample thickness. The cross section images show the effect of the radial distribution of shear rate on the radial distribution of morphology; the result for the case considered in Fig. 3 (shearing time of 10 s with shear rate of 5 s^{-1}) is shown in Fig. 4. It is clear from the micrographs that the dimensions of the spherulites decrease on increasing the distance from the center, namely on increasing the shear rate.

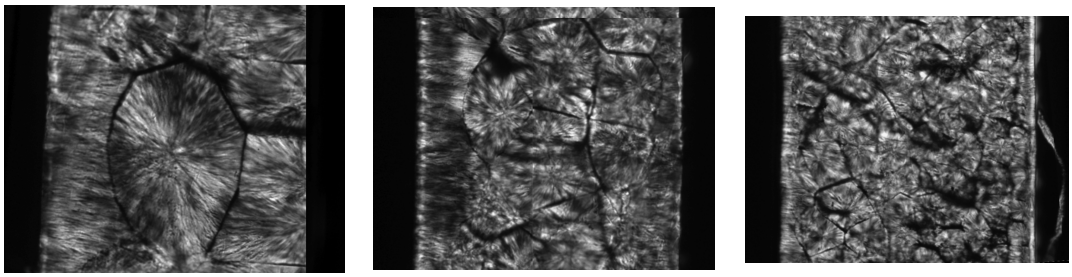

a b C

Fig. 4 Polarized optical micrographs of the solidified and sectioned sample, shear rate 5 s^{-1} and shearing time 10 s, at three distances from the center a) R = 0 mm, b) R= 5.5 mm, and c) R= 9 mm The sample section is 500 µm thick.

A significant spherulite nucleation at the quartz surface was observed, consistently with previous literature reports [41]; surface nucleated structures presented dimensions of the order of the spherulite radii observed in the core at corresponding position.

The effect of different shearing times on the morphology of the spherulitic structure after crystallization is shown in Fig. 5, as final diameter, *D*. This mean diameter is evaluated, with error bars, smoothing hundreds of spherulites measurements, on each sectioned sample, with FFT filtering.

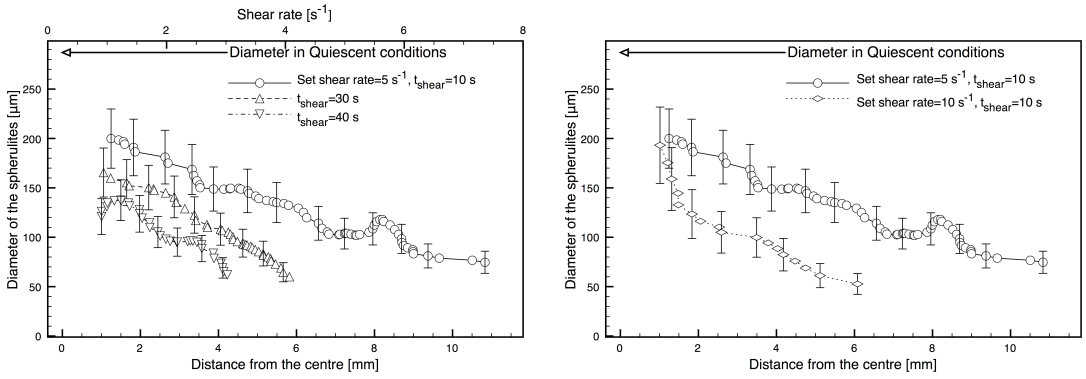

a B

Fig. 5 Diameter (left) as function of the radial distribution of shear rate from experiments with: a) shear rate 5 s^{-1}, shearing time 10, 30 and 40 s; b) shearing time 10 s and shear rate 5 s^{-1} and 10 s^{-1}; the arrow on the top of the plots indicates the diameter reached by the spherulites in quiescent conditions, at 140°C.

For each shearing time, the final spherulite radius clearly decreases with shear rate and in general also with the time of the shear step. This is consistent with a nucleation rate increasing with the shear rate during the shear step, its effect indeed increases with the shear time and, for a given time, with the local shear rate. Obviously, a larger number of nuclei gives rise to smaller spherulites.

Delayed **step shear**

With the *delayed* protocol the shear step is applied when the spherulites are already detectable by microscopic observations after nucleation and growth in quiescent conditions, i.e. after about 15-20 min at 140°C.

This protocol can be adopted for measuring both the nucleation and the growth rate during shear, even at moderate shear rates. An example of the results which can be obtained is reported in Figs. 6 and 7, which show pictures taken soon before and soon after the shear steps. At the beginning of the shear step, the spherulites are big enough to focus clearly on them, and it is also possible to identify a spherulite close to the fixed plate, so that it does not move significantly during shear. It is worth mentioning that in all the experiments performed in this work the crystalline structures keep a spherical shape, without any preferential growth along a particular direction

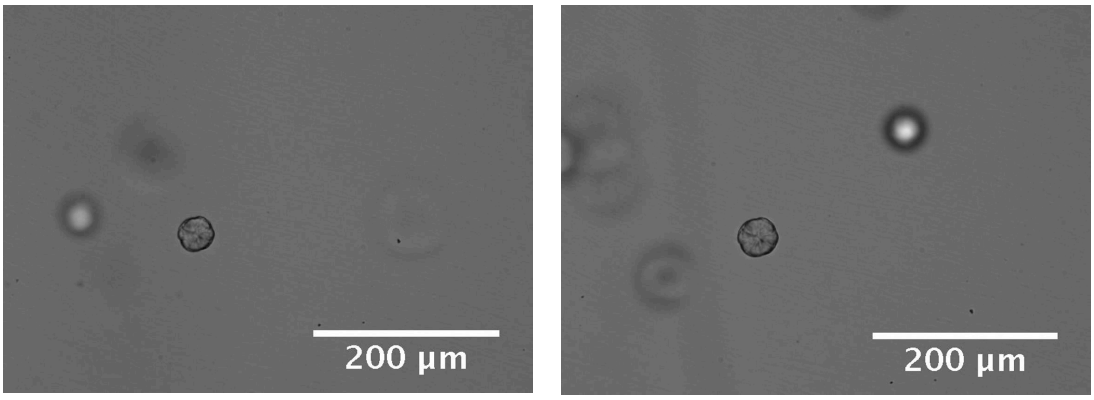

a b

Fig. 6. Pictures taken soon before (a) and soon after (b) a delayed step shear of 200 s at a shear rate of 0.2 s^{-1}.

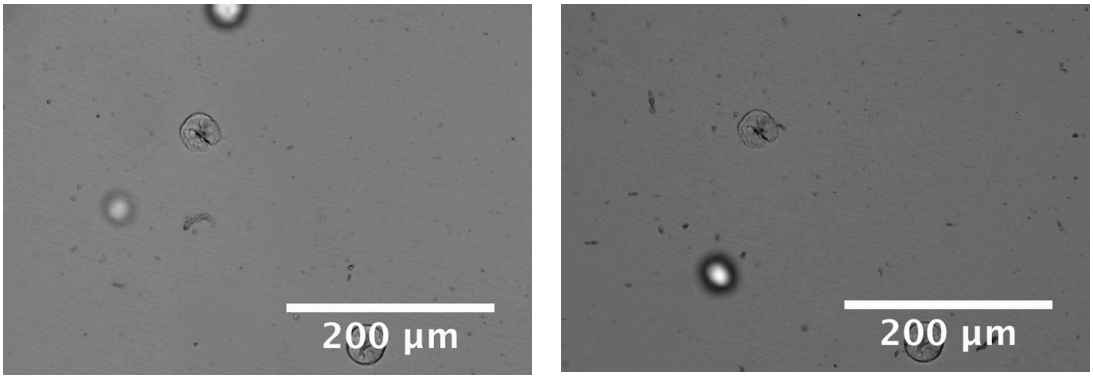

a b

Fig. 7. Pictures taken soon before (a) and soon after (b) a delayed step shear of 10 s at a shear rate of 2 s^{-1}.

The growth of the spherulites could thus be monitored during the shear steps as shown in Fig. 8 and the growth rate was evaluated.

The data of radius evolution, similar to those reported in Fig. 8, showed very interesting characteristics:

- as expected, before the application of the flow, the growth rate (namely the slope of the plot reporting the radius versus time) corresponds to the values measured in quiescent conditions and reported in the literature, about $G_{quiescent}$=7×10^{-3} µm/s [5, 32], for the same material at the same temperature, T=140°C;
- at the application of the flow, the growth rate immediately changes assuming a higher value, which is found constant until the shear rate is constant; this means that the material immediately adjusts to the new flow conditions, with a reaction time surely lower than half a second;
- as soon as the shear rate is released, the growth rate returns back to the quiescent value. Again, the adjustment to the new condition was found faster than measurable with the adopted technique.

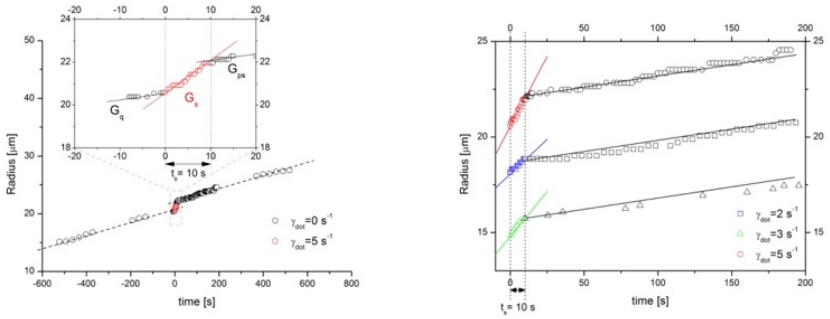

Fig. 8 Spherulite radius evolution for shear rate 5 s^{-1}, shearing time 10 s (left) and for shear rates 2, 3 and 5 s^{-1}, shearing time 10 s (right).

The collected data of growth rate analyzed in this work are reported in Fig. 9. All the data reported in Fig. 9 show that an increase of shear rate induces an increase of growth rate. Also literature data collected on the same material [37] at the same temperature but at lower and continuous shear rates are reported in the Fig. 9. It can be noticed that a much wider range of shear rates could be explored in this work, because of the potentialities achieved with the *delayed* protocol. Furthermore, it can be stated that the data collected in this work (with the *delayed* protocol) are much more reliable even at low shear rates, since as stated above, on increasing the shear rate the uncertainties in the measurement of growth rate taken with continuous and *immediate* shear protocol are quite large.

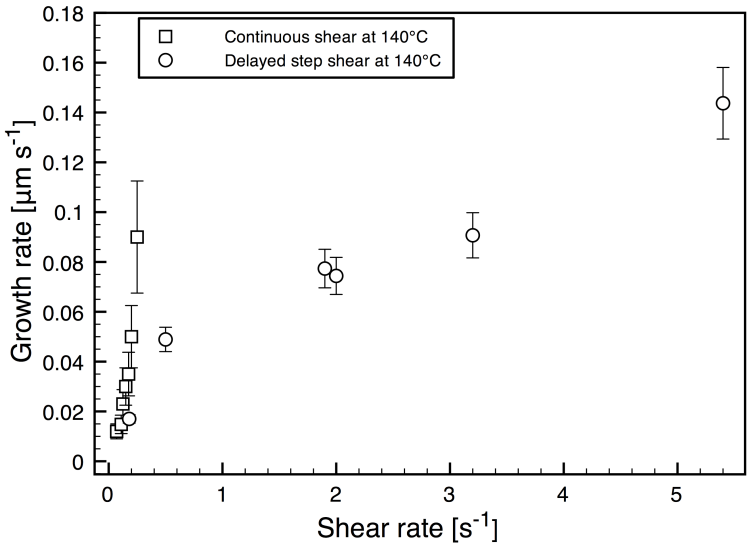

Fig. 9 Growth rate evaluated from radii evolution during delayed step shear and continuous shear [37].

Discussion

Nucleation rate

The "*delayed"* shear step protocol is also suitable for estimating the nucleation rate, because the spherulites born during the shear step can be clearly identified through their dimensions. As an example, in Fig. 10 a picture taken 800 s after a shear step carried out with a shear rate of 2 s^{-1} and for 40 s is reported. It can be clearly seen that two populations of spherulites are present: larger ones, which were already large during the quiescent period of 20 min, and smaller ones, which were instead born during the shear step. It is therefore possible, from the pictures collected after the *delayed* shear step, to count the spherulites composing this latter population and, dividing the result by the shearing time, calculate the nucleation rate. These values of nucleation rate, calculated from the *delayed* experiments, neglect the nucleation rate after cessation of flow, however this effect should be very small if the nucleation rate follows the growth rate which, as observed in the previous section, during *delayed* step shear experiments returns to its quiescent value as soon as the step shear ends.

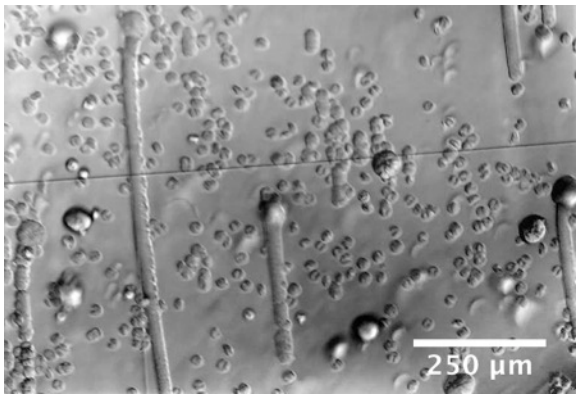

Fig. 10 Picture taken 800 s after a shear step carried out with a shear rate of 2 s^{-1} and for 40 s.

The nucleation rate under shear was evaluated also from the experiments carried out with the *immediate* step shear protocol both by dividing the optical observations of nucleation density at the optical window by the shearing time, and from the final average diameters of spherulites reported in Fig. 5. Indeed, assuming that during the shear step, for the

conditions applied, the volume occupied by crystals is negligible and that all the formed nuclei are active, namely will generate a spherulite, the density of active nuclei is just related to the final average diameter of the spherulites, reported in Fig. 5, by the following simple relationship:

$$N_V = 6/\pi D^3 \tag{2}$$

and thus the nucleation rate can be obtained by dividing the results of the previous equation by the shearing time under the hypothesis that, similarly to what observed with the growth rate, the nucleation rate is constant during the shearing time. This gives

$$\dot{N} = \left(N_V - N_Q\right)/t_{shear} \tag{3}$$

where N_Q is the predetermined density of nuclei present in quiescent conditions, which for the selected material at 140°C is about 8×10^{-8} nuclei μm^{-3} [32].

All values of nucleation rate calculated by both delayed and immediate experiments, from windows observation and from final average spherulite diameters are reported in Fig. 11; also literature data [37, 39] obtained from continuous shear experiments are there reported for comparison.

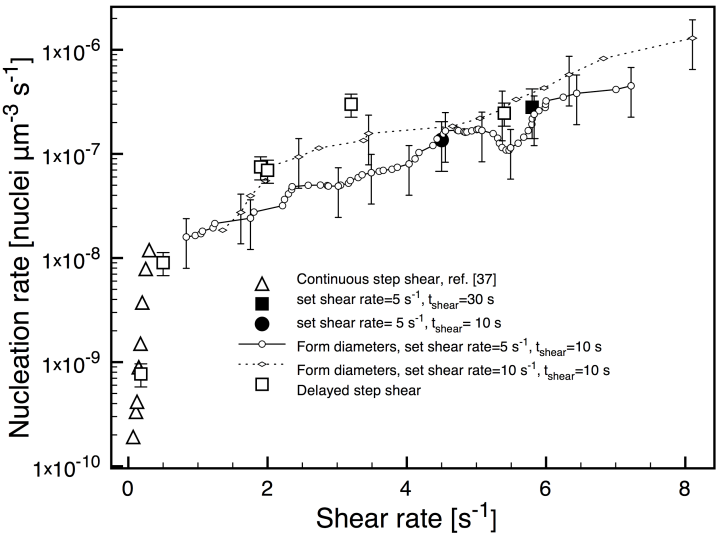

Fig. 11. Nucleation rate evaluated from different experiments vs shear rate.

The plot reported in Fig. 11 certainly shows that the nucleation rate is correlated to the shear rate. Although at each shear rate larger than about 1 s^{-1}, the ensemble of all the series of data spans over about half a decade on the nucleation rate scale, the data clearly show that the correlation is roughly composed of two linear zones in the semi log plot of the figure. At the knee, taking place at about 0.3 s^{-1}, the slope undergoes a sharp decrease by a factor of about 20.

It is worth mentioning that for all the data presented in this work a spherulitic regime is found. On the basis of previous results [42] it is reasonable to suppose that the range of shear rates explored covers most of this regime: higher shear rates would induce the fibrillar morphology.

Growth rate

In a previous work [37], it was found that, nucleation rate and spherulitic growth rate are tightly correlated. Furthermore, it was shown that in quiescent condition the nucleation rate was not measurable. Consistently, in this work, an attempt was made to correlate the nucleation rate to the excess growth rate of the spherulites during flow, namely versus G-$G_{quiescent}$,where $G_{quiescent}$ is the growth rate of the spherulites in quiescent conditions. according to the Hoffman and Lauritzen equation $G_{quiescent}$ depends on the temperature as follows

$$G(T) = G_0 \exp\left[-\frac{U/R}{T-T_\infty}\right]\exp\left[-\frac{K_g\left(T+T_m^0\right)}{2T^2\left(T_m^0-T\right)}\right] \qquad (4)$$

The parameters to be adopted in eq. 4 for the i-PP adopted in this work are reported in Table 2.

Table 2. Values of the parameters adopted to describe the experimental data of quiescent spherulitic growth rate as identified in a previous work [37].

	G_0 [μm s^{-1}]	U/R [K]	K_g [K^2]	T_∞ [°C]	T_m^0 [°C]
Regime III, T<137°C	2.9 10^{10}	751.6	534858	-37.2	194
Regime II, T>137°C	1.7 10^5	751.6	267429	-37.2	194

Two regimes of the growth rate kinetics where identified , each of which was characterized by different values of the two parameters K_g and G_0, as specified in Table 2. In previous papers considering the crystallization kinetics of the material adopted in this work, the experimental temperature dependence of the growth rate was described by eq. 4 and the effect of flow on growth rate was ascribed only to the equilibrium melting temperature T_m^0. The increase of T_m^0 in eq. 4 determines an increase of the growth rate; for each T_m^0 the change of regime takes place at the temperature at which the two regimes give rise to the same growth rate, this happens at 137°C under quiescent conditions.

If T_m^0 increases, by effect of the flow, the crystallization regime changes again at the temperature at which both regimes (defined by the constants reported in Table 2) give rise to the same growth rate and this happens when

$$T_m^0 = T\frac{\left(2AT^2+1\right)}{\left(2AT^2-1\right)} \quad \text{where} \quad A = \left(K_g^{II}-K_g^{III}\right)^{-1}\ln\left(G_0^{II}\Big/G_0^{III}\right) \qquad (5)$$

Replacing T_m^0 as given by eq. 5 into eq. 4 one obtains the growth rate $G_t(T)$ at the transition between the two regimes

$$G_T(T) = G_0^{II}\exp\left[-\frac{U/R}{T-T_\infty}\right]\exp\left[-K_g^{II}A\right] = G_0^{III}\exp\left[-\frac{U/R}{T-T_\infty}\right]\exp\left[-K_g^{III}A\right] \qquad (6)$$

The resulting plot is shown in Fig. 12, in which the dashed line identifies the change of crystallization regime and corresponds to eq. 6.

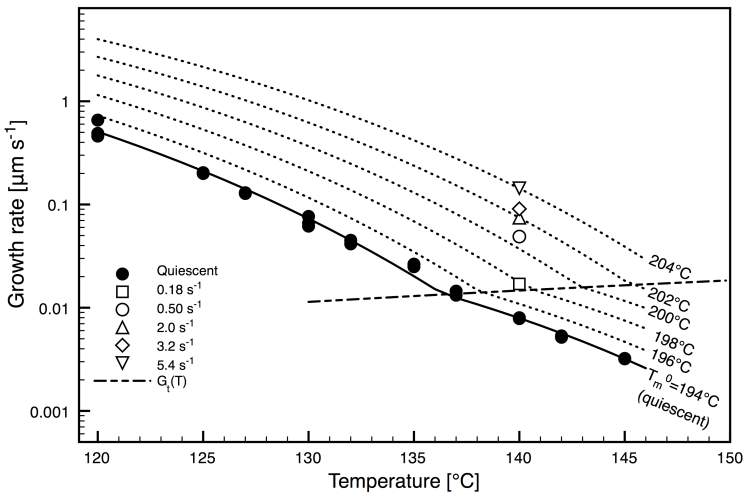

Fig. 12. Results of growth rate in quiescent conditions (filled circles) and during shear flow. Dotted lines are obtained by changing the equilibrium melting temperature in eq. 4. The dashed line identifies the change of growth regime.

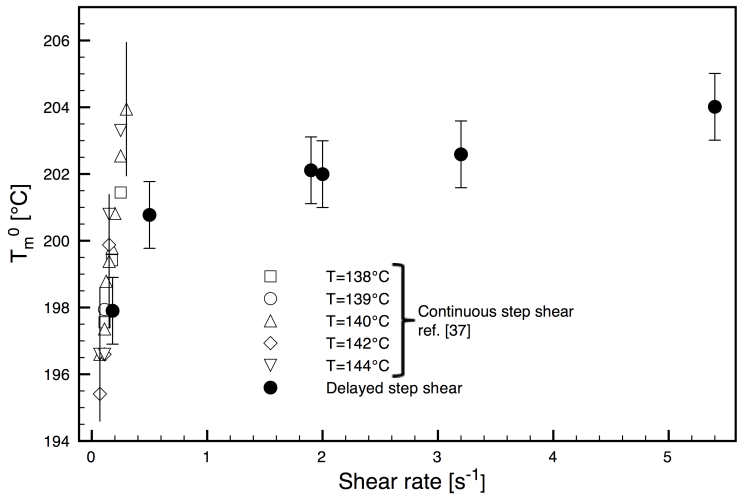

Fig. 13. Equilibrium melting temperature, T_m^0 in eq. 4, as a function of shear rate. Data collected during continuous shear rate (empty symbols) are taken from literature [37].

For each temperature and shear rate, the values of the equilibrium melting temperature T_m^0, which should be adopted in eq. 4 (or in Fig. 12), in order to obtain the value of spherulite growth rate measured experimentally is plotted in Fig. 13 versus the shear rate. Also the results obtained in the previous work [37] are plotted in Fig. 13 for comparison.

The obtained plot consists essentially of two straight segments, the first one at very low shear rates (up to about 0.3 s^{-1}) has a slope of about 20°C s, whereas the second straight line which holds at higher shear rates has a slope about 30 times smaller.

Growth rates are available only for the experiments carried out with the *delayed* protocol and for those reported in a previous work [37]. Corresponding nucleation rates are reported in Fig. 14 versus the data of excess growth rate. Fig. 14 confirms that there is a correlation between nucleation rate and excess spherulitic growth rate, at all the temperatures and shear rates considered. At the largest excess growth rates, namely at the largest applied shear rates, the new data

present nucleation rates larger with respect to the older data. This could again be ascribed to the difficulties in determining the growth rate with the older protocol.

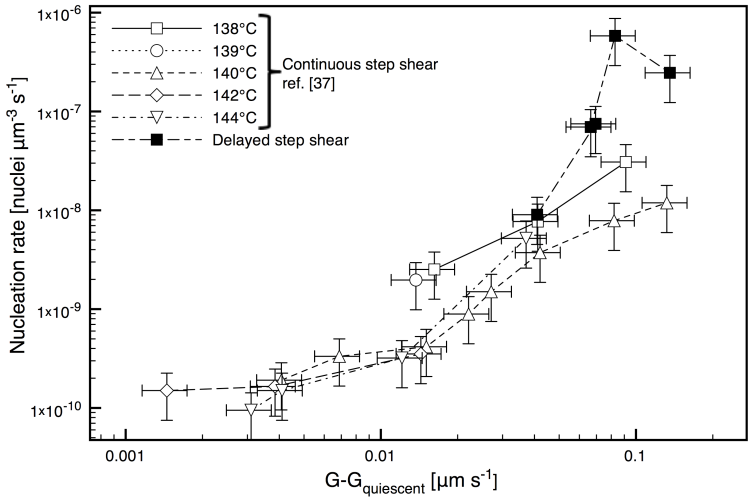

Fig. 14 Nucleation rate versus excess growth rate for i-PP under several temperature and shear rate conditions.

Both growth and nucleation rates can be obtained from the combined use of Figs. from 12 to14, obviously for the resin studied in this work and in the ranges of temperatures and shear rates considered in the experiments.

Indeed in sequence, once the shear rate is known, the equilibrium melting temperature T_m^0 can be calculated from Fig. 13; once T_m^0 has been determined, and the temperature has been specified, the growth rate is determined by Fig. 12 and the nucleation rate by Fig. 14, within its approximation.

Conclusions

In this work, step shear tests were conducted in the Linkam shearing device in order to study the effect of flow on the evolution of morphology during crystallization.

Delaying the flow start of a time sufficient to let nuclei born under quiescent conditions to reach dimensions easily detectable by an optical microscope allowed to achieve a more careful and accurate experimental analysis of the effect of flow on spherulite growth rate. With such a *delayed* protocol it could be experimentally clarified that, for the resin adopted in this work, the spherulitic growth rate changes by effect of a shear rate change (either an increase or a decrease) following nearly immediately the changes of shear rate during step shear experiments. Furthermore, the increase of accuracy achieved by the *delayed* protocol in the analysis of the effect of flow on spherulites growth rate allowed to increase of one order of magnitude the experimental shear rate range with respect to the previous literature.

Results taken from the literature and new results on the same i-PP grade were interpreted on the basis of Hoffman-Lauritzen equation for spherulitic growth rate, with the equilibrium melting temperature T_m^0 function of the shear rate, the functionality being experimentally determined.

Also the nucleation rate was analyzed by two methods: from the morphology evolution optically monitored during crystallization (after both *delayed* and *immediate* protocols); and from the average spherulitic radius in the samples solidified under constant temperature after the shear steps. The results, including literature ones, confirm the existence

of a correlation between the nucleation rate and the shear rate and furthermore between nucleation rate and growth rate under the same shear rate.

The morphology monitored during the *delayed* shear step protocol reveal a significant higher value of the nucleation rate with respect to previous data under the same shear rate range.

The experimental data of morphology evolution are organized into a set of plots that adopted in the proper sequence allow to evaluate both growth and nucleation rates in the ranges of temperatures and shear rates considered in the experiments.

References

1. Housmans J-W, Gahleitner M, Peters GW, and Meijer HE. Polymer 2009;50(10):2304-2319.
2. Menyhárd A, Gahleitner M, Varga J, Bernreitner K, Jääskeläinen P, Øysæd H, and Pukánszky B. European Polymer Journal 2009;45(11):3138-3148.
3. van Drongelen M, Gahleitner M, Spoelstra AB, Govaert LE, and Peters GW. Journal of Applied Polymer Science 2015;132(23).
4. Janeschitz-Kriegl H. Crystallization modalities in polymer melt processing: Springer, 2009.
5. De Santis F, Vietri AR, and Pantani R. Morphology evolution during polymer crystallization simultaneous calorimetric and optical measurements. Macromolecular symposia, vol. 234: Wiley Online Library, 2006. pp. 7-12.
6. Somani RH, Yang L, Hsiao BS, Agarwal PK, Fruitwala HA, and Tsou AH. Macromolecules 2002;35(24):9096-9104.
7. Haas TW and Maxwell B. Polymer Engineering & Science 1969;9(4):225-241.
8. Mackley M and Keller A. Polymer 1973;14(1):16-20.
9. Sherwood C, Price F, and Stein R. Effect of shear on the crystallization kinetics of poly (ethylene oxide) and poly (e-caprolactone) melts. Journal of Polymer Science: Polymer Symposia, vol. 63: Wiley Online Library, 1978. pp. 77-94.
10. Ulrich RD and Price FP. Journal of Applied Polymer Science 1976;20(4):1077-1093.
11. Pogodina NV, Lavrenko VP, Srinivas S, and Winter HH. Polymer 2001;42(21):9031-9043.
12. Koscher E and Fulchiron R. Polymer 2002;43(25):6931-6942.
13. Fiorentino B, Fulchiron R, Duchet-Rumeau J, Bounor-Legaré V, and Majesté J-C. Polymer 2013;54(11):2764-2775.
14. Devaux N, Monasse B, Haudin J-M, Moldenaers P, and Vermant J. Rheologica acta 2004;43(3):210-222.
15. Tavichai O, Feng L, and Kamal MR. Polymer engineering and science 2006;46(10):1468.
16. Mykhaylyk OO, Chambon P, Graham RS, Fairclough JPA, Olmsted PD, and Ryan AJ. Macromolecules 2008;41(6):1901-1904.
17. Mykhaylyk OO, Chambon P, Impradice C, Fairclough JPA, Terrill NJ, and Ryan AJ. Macromolecules 2010;43(5):2389-2405.
18. Najafi N, Heuzey M-C, Carreau P, and Therriault D. Rheologica acta 2015;54(9-10):831-845.
19. Kumaraswamy G, Verma RK, and Kornfield JA. Review of scientific instruments 1999;70(4):2097-2104.
20. Kumaraswamy G, Issaian AM, and Kornfield JA. Macromolecules 1999;32(22):7537-7547.
21. Kumaraswamy G, Verma R, Issaian A, Wang P, Kornfield J, Yeh F, Hsiao B, and Olley R. Polymer 2000;41(25):8931-8940.
22. Kumaraswamy G, Kornfield JA, Yeh F, and Hsiao BS. Macromolecules 2002;35(5):1762-1769.
23. Kornfield JA, Kumaraswamy G, and Issaian AM. Industrial & engineering chemistry research 2002;41(25):6383-6392.
24. Swartjes FHM, Peters GW, Rastogi S, and Meijer HE. International Polymer Processing 2003;18(1):53-66.
25. Housmans J-W, Balzano L, Santoro D, Peters G, and Meijer H. International Polymer Processing 2009;24(2):185-197.
26. Custódio FJ, Steenbakkers RJ, Anderson PD, Peters GW, and Meijer HE. Macromolecular Theory and Simulations 2009;18(9):469-494.
27. Troisi E, Portale G, Ma Z, van Drongelen M, Hermida-Merino D, and Peters G. Macromolecules 2015.
28. Ma Z, Balzano L, Portale G, and Peters GW. Polymer 2014;55(23):6140-6151.
29. Mackley M, Marshall R, and Smeulders J. Journal of Rheology (1978-present) 1995;39(6):1293-1309.
30. Mackley M and Hassell D. Journal of Non-Newtonian Fluid Mechanics 2011;166(9):421-456.
31. Zhang C, Hu H, Wang D, Yan S, and Han CC. Polymer 2005;46(19):8157-8161.
32. Coccorullo I, Pantani R, and Titomanlio G. Polymer 2003;44(1):307-318.
33. De Santis F, Lamberti G, Peters GW, and Brucato V. European polymer journal 2005;41(10):2297-2302.

34. Pantani R, Coccorullo I, Speranza V, and Titomanlio G. Progress in polymer science 2005;30(12):1185-1222.
35. Pantani R, Coccorullo I, Speranza V, and Titomanlio G. Polymer 2007;48(9):2778-2790.
36. Coccorullo I, Pantani R, and Titomanlio G. Macromolecules 2008;41(23):9214-9223.
37. Pantani R, Coccorullo I, Volpe V, and Titomanlio G. Macromolecules 2010;43(21):9030-9038.
38. Pantani R, Speranza V, Coccorullo I, and Titomanlio G. Morphology of injection moulded iPP samples. Macromolecular Symposia, vol. 185: Wiley-Blackwell, 111 River Street Hoboken NJ 07030-5774 USA, 2002. pp. 309-326.
39. LinkamScientific.
40. De Santis F, Scermino R, Pantani R, and Titomanlio G. Spherulitic nucleation and growth rates in a sheared polypropylene melt. PROCEEDINGS OF PPS-29: The 29th International Conference of the Polymer Processing Society-Conference Papers, vol. 1593: AIP Publishing, 2014. pp. 294-297.
41. Nowacki R, Monasse B, Piorkowska E, Galeski A, and Haudin J. Polymer 2004;45(14):4877-4892.
42. Pantani R, Nappo V, De Santis F, and Titomanlio G. Macromolecular Materials and Engineering 2014;299(12):1465-1473.